Environ Sci Pollut Res (2018) 25:23451–23467
DOI 10.1007/s11356-016-7096-0

Estimating ecosystem metabolism from continuous multi-sensor measurements in the Seine River

N. Escoffier[1,5,6] · **N. Bensoussan**[2] · **L. Vilmin**[3,7] · **N. Flipo**[3] · **V. Rocher**[4] · **A. David**[5] · **F. Métivier**[1] · **A. Groleau**[1]

Received: 28 February 2016 / Accepted: 13 June 2016 / Published online: 22 June 2016

Abstract Large rivers are important components of the global C cycle. While they are facing an overall degradation of their water quality, little remains known about the dynamics of their metabolism. In the present study, we used continuous multi-sensors measurements to assess the temporal variability of gross primary production (GPP) and ecosystem respiration (ER) rates of the anthropized Seine River over an annual cycle. Downstream from the Paris urban area, the Seine River is net heterotrophic at the annual scale (−226 $gO_2\ m^{-2}\ year^{-1}$ or −264 $gC\ m^{-2}\ year^{-1}$). Yet, it displays a net autotrophy at the daily and seasonal scales during phytoplankton blooms occurring from late winter to early summer. Multivariate analyses were performed to identify the drivers of river metabolism. Daily GPP is best predicted by chlorophyll *a* (Chl*a*), water temperature (*T*), light, and rainfalls, and the coupling of daily GPP and Chl*a* allows for the estimation of the productivity rates of the different phytoplankton communities. ER rates are mainly controlled by *T* and, to a lesser extent, by Chl*a*. The increase of combined sewer overflows related to storm events during the second half of the year stimulates ER and the net heterotrophy of the river. River metabolism is, thus, controlled at different timescales by factors that are affected by human pressures. Continuous monitoring of river metabolism must, therefore, be pursued to deepen our understanding about the responses of ecosystem processes to changing human pressures and climate.

Keywords Continuous monitoring · River metabolism · Primary production · Ecosystem respiration · Phytoplankton · Urban pressures

Introduction

Freshwater ecosystems are undergoing increasing anthropogenic pressures through growing population density, land use conversion, and associated global climate change (Millenium Ecosystem Assessment 2005). While management policies

Responsible editor: Philippe Garrigues

Electronic supplementary material The online version of this article (doi:10.1007/s11356-016-7096-0) contains supplementary material, which is available to authorized users.

✉ N. Escoffier
nicolas.escoffier@epfl.ch

[1] Institut de Physique du Globe de Paris, Sorbonne Paris Cité, Université Paris Diderot, UMR 7154 CNRS, 75005 Paris, France

[2] IPSO-FACTO, SCOP arl, Pôle Océanologie et Limnologie, 10, rue Guy Fabre, 13001 Marseille, France

[3] Mines ParisTech, PSL Research University, Centre de Géosciences, 35, rue Saint-Honoré, 77305 Fontainebleau, France

[4] Syndicat Interdépartemental pour l'Assainissement de l'Agglomération Parisienne, Direction du Développement et de la Prospective, 82 avenue Kléber, 92700 Colombes, France

[5] Nke Instrumentation, Z.I. de Kérandré, rue Gutenberg, 56700 Hennebont, France

[6] Present address: Stream Biofilm and Ecosystem Research Laboratory, Ecole Polytechnique Fédérale de Lausanne (EPFL), Station 2, CH-1015 Lausanne, Switzerland

[7] Present address: Department of Earth Sciences—Geochemistry, Faculty of Geosciences, Utrecht University, Utrecht, The Netherlands

are developed throughout the world to assess the quality of these ecosystems, most studies of ecosystem functioning are based on structural descriptive metrics such as water chemistry or biological community composition (Bott et al. 2006). The importance of ecosystem function in assessing the ecologic status of aquatic ecosystems (Vighi et al. 2006) is stated within the European Water Framework Directive (WFD, EC 2000/60/CE) but the implementation of functional indicators in monitoring programs remains scarce (Young et al. 2008).

Among functional metrics, the components of ecosystem metabolism (i.e., GPP and ER) provide direct metrics to assess the balance of allochtonous and autochtonous organic matter sources, C fluxes, and the trophic structure of aquatic ecosystems (Dodds and Cole 2007). Initially conceptualized from diel dissolved oxygen (DO) variations of flowing waters (Odum 1956), this approach has later been adapted to different types of aquatic ecosystems. Most of the scientific studies have focused on lakes (Staehr et al. 2010) and streams (Aristegi et al. 2009; Bernot et al. 2010). Yet, our knowledge on large river metabolism remains limited (Hall et al. 2015). Rivers, but also lakes and wetlands, are largely contributing to the global C cycle. Recent references reported overall estimates of 1.2 to 1.8 PgC $year^{-1}$ released to the atmosphere as CO_2 and 0.9 PgC $year^{-1}$ transported to oceans as organic and inorganic C (Aufdenkampe et al. 2011; Raymond et al. 2013). Even though rivers and streams only represent 0.47 % of the Earth's surface (Raymond et al. 2013), the amount of C emitted to the atmosphere or buried in sediments in these systems is of the same order of magnitude as the fluxes assigned to marine and terrestrial sequestration, respectively (Battin et al. 2009; Tranvik et al. 2009). In the case of rivers, these observations support the River Continuum Concept (RCC) in the fact that these systems are heterotrophic on an annual basis (Vannote et al. 1980). However, the RCC also states that phytoplankton communities are important actors in high-order river (>5th order) metabolism and that autotrophy may be significant at shorter time scales. To date, few references support this statement (e.g., Dodds et al. 2013; Hall et al. 2015), and most of the lotic ecosystem metabolism studies are performed from short-term measurements during stable discharge conditions in one or two seasons (Mulholland et al. 2001; Bernot et al. 2010).

Recent improvements in sensor technology allow continuous measurements of ecosystem metabolism over large spatial and temporal scales. Despite this significant technological breakthrough, references on the use of these methods for the monitoring of lotic ecosystems remain scarce (Roberts et al. 2007; Beaulieu et al. 2013), particularly for rivers (Vink et al. 2005; Uehlinger 2006). The challenges mainly lie in the complexity of river ecosystems and the confounding effects of hydraulic and physical processes on the variations of DO. To overcome these limitations, Bayesian statistical approaches have been applied in a few rivers and estuaries studies (Holtgrieve et al. 2010; Riley and Dodds 2013). However, the results remain dependent on the uncertainties associated to a proper mathematical forward modeling of ecosystem processes.

Albeit large river systems process large carbon fluxes and are very often subject to significant anthropogenic pressures, continuous data that permit to estimate their metabolism are usually missing. The urban stream syndrome has recently been proposed to summarize the impacts of urban areas on stream water quality (Walsh et al. 2005). Yet, no clear consensus has emerged regarding the corresponding effects on functional metrics such as ecosystem metabolism (Wenger et al. 2009). Further investigations are, therefore, required to assess these effects, particularly in the context of large flowing systems.

In this study, we focus on the downstream part of the Seine River, which is impacted by upstream agricultural practices on its watershed and the immediate influence of effluents from the Paris urban area (Garnier and Billen 2007). Multiparameter monitoring stations were deployed in the river, and the corresponding continuous measurements were analyzed to address the following objectives:

(1) to show that multi-sensor monitoring stations are appropriate to estimate the metabolism of large rivers under high urban pressures;
(2) to identify the drivers of the different components of the river metabolism and determine their relative timescales of influence;
(3) to compare the identified patterns with the predictions of the RCC and with the results reported for other types of lotic ecosystems, in order to highlight the specificities of such large anthropized river system.

Material and methods

Study area

The drainage area of the Seine River watershed covers an area of 78,600 km^2, that mainly corresponds to the Paris Basin (Fig. 1). Its hydrological regime is pluvio-oceanic, with an average rain precipitation of 750 mm $year^{-1}$. The Seine basin is divided into major Hydro-Eco-Regions (HER) based on the lithology (mainly calcareous), the land-use and the population density (Garnier and Billen 2007). The study area is integrated in the Ile-de-France HER, whose surface area of 18,478 km^2 hosts a mean population density of 977 inhabitants km^{-2}.

This work addresses the Seine River in its urban part, downstream from the Paris area. According to Strahler's ordination (Strahler 1957), the Seine River is classified as a seventh-order stream from its confluence with the Marne

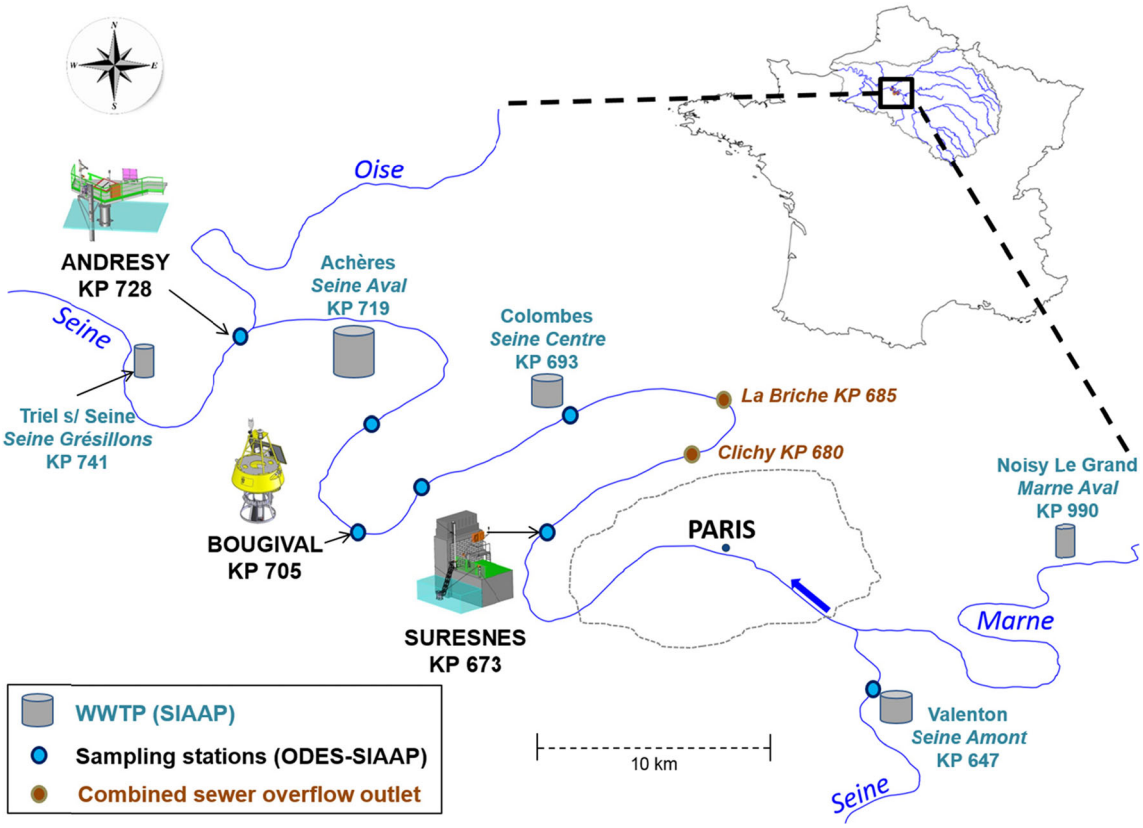

Fig. 1 The Seine River watershed, the study area downstream Paris and locations of Suresnes, Bougival and Andrésy stations of the CarboSeine network. *WWTP*: wastewater treatment plant, *KP*: kilometric point from source of the Seine River

River, upstream from Paris, to its confluence with the Oise River, 70 km downstream from Paris (Fig. 1). The mean discharge of the river in Paris is about 330 $m^3\ s^{-1}$. The river bed has been channelized and constrained since the nineteenth century. The construction of specific reservoirs upstream Paris in the second half of the twentieth century allowed regulating the flood effects and sustaining the summer flow around 100 $m^3\ s^{-1}$ in Paris (Garnier et al. 1995). The Greater Paris area concentrates two thirds of the Seine basin population (i.e., 11 million inhabitants), whose domestic effluents are treated in four waste–water treatment plants (WWTP) monitored by the institution in charge (Syndicat Interdépartemental pour l'Assainissement de l'Agglomération Parisienne, SIAAP). Actually, during severe rainy events, the transport capacity of the sewer system may be insufficient and combined sewer overflow (CSO) water, composed of urban runoff and wastewater, are discharged directly into the Seine River. The Clichy and La Briche outlets (Fig. 1) account for about 30 to 60 % of the annual discharge of such storm events.

The continuous data used in this study were recorded during the year 2011 at the Bougival monitoring station of the CarboSeine network, which is deployed downstream from the main WWTP and CSO outlets of the area (Fig. 1). At this location, the Seine's water depth is about 4.3 m.

Continuous multi-parameter measurements

The CarboSeine station at Bougival is composed of various sensors, which record water stage, *T*, pH, turbidity, specific conductivity (C_{25}), DO concentrations (multi-parameter Mp6 probe, Nke Instrumentation, France), total phytoplanktonic Chl*a* (FluoroProbe series 2, bbe Moldaenke GmbH, Schwentinental, Germany), solar irradiance (CMP 11 series, Kipp & Zonen, Delft, Netherlands) and meteorological parameters (WXT-520 series, Vaisala, Vantaa, Finland) every 15 min. Additional sensors are also deployed punctually to perform complementary high-frequency sampling, such as soluble-reactive phosphate (SRP) by in situ colorimetric assessment every 2 h (Cycle P, Wetlabs, Philomath, OR, USA). The data are collected and stored by an automated central datalogger (Abin Series, Nke Instrumentation, Hennebont, France) and subsequently GPRS-transmitted towards a specific database (http://carboseine.ipgp.fr). Adapted filtering procedures are used for partial automatic validation of the data, which can further be processed and exported by operators. The dataset considered in this study was recorded from 1st of January to 31st of December 2011.

Dissolved oxygen and physico-chemical parameters

DO was measured using a nke-Mp6 probe with optical DO sensor (Optode 4830 series, Anderaa Instruments, Nesttun, Norway). Prior to the deployment of the sensor, DO calibration was performed using the water-saturated air method. Zero percent saturation was calibrated in 10 g L^{-1} Na_2SO_3 solution. In situ metrology of DO, *T*, C_{25}, and pH was verified monthly to bi-monthly during field campaigns, by comparison with the data provided by an independent multi-parameter probe (Multi-3430, set WTW). Additionally, DO concentrations were measured on discrete field samples by the Winkler method (Winkler 1888), with an average precision of 1 %. Potential DO calibration drifts were thus cautiously checked, but no data correction was necessary. DO theoretical saturation was calculated from *T*, salinity, and barometric pressure (Benson and Krause 1984).

Chlorophyll a

Chl*a* concentrations were measured using an in situ multi-wavelength fluorometer. The FluoroProbe (FP) measures total phytoplanktonic biomass (expressed in microgram of Chl*a* per liter) and parses it among four algal groups (i.e., "green" (Chlorophyta and Euglenophyta), "blue" (Cyanophyta), "brown" (Bacillariophyta, Dinophyta, Chrysophyta) and "red" (Cryptophyta)) on the basis of their fluorescence excitation spectra (Catherine et al. 2012). Prior to its deployment, the FP was calibrated with two species of Bacillariophyta and Chlorophyta (i.e., *Nitzschia palea* (Kützing) W. Smith and *Pediastrum boryanum* (Turpin) Meneghini) representative of the phytoplankton communities of the Seine River. Spectral fluorescence signatures (SFS) were defined for the two species and activated within the device after verifying their linear independence towards other activated SFS (Escoffier et al. 2015). In order to assess the device's calibration, grab samples were collected at a monthly to bi-monthly frequency to measure Chl*a* concentrations and perform phytoplankton cell enumerations and biovolume measurements.

Discharge and CSO inputs

The discharge data was provided by the DIREN–Ile-de-France and recorded every 10 min at the Austerlitz bridge in Paris. This data was used to back-calculate discharge and water velocities at Bougival according to the relationships implemented in the ProSe numerical model. This model simulates the hydraulic and biogeochemical processes in the Seine River from the Paris urban area to the entrance of the estuary (Even et al. 2004; 2007; Vilmin et al. 2015). Daily CSO inputs at the main outlets were provided by the SIAAP.

River metabolism assessment

Metabolism assessment was based on the single station diel oxygen approach (Odum 1956) and adapted according to recent improvement procedures (Staehr et al. 2010; Needoba et al. 2012). Metabolism estimates were calculated from continuous DO, *T*, irradiance, water and wind velocity data. The mass balance equation governing instantaneous DO rate of change is written as follows:

$$\frac{\mathrm{dC}}{\mathrm{dt}} = \mathrm{GPP}(t) + F(t) - \mathrm{ER}(t) \pm A(t)$$

The advection term $A(t)$ integrates changes in the water body due to transport from external sources (Cox 2003), such as hyporheic surface-groundwater exchange (Hall and Tank 2005). Due to channelization of the river bed, such processes are unlikely to happen in this river stretch. $A(t)$ is therefore neglected. In case of significant lateral inputs, the compliance of corresponding metabolic estimates to the single station hypothesis of water masses homogeneity was cautiously checked. $F(t)$ is the rate of DO exchange with the atmosphere, also called piston velocity, and is calculated as:

$$F(t) = \frac{K}{h}(\mathrm{Cs}(t) - C(t))$$

where $C(t)$ is the instantaneous DO concentration, $\mathrm{Cs}(t)$ is the saturating DO concentration, K is the reaeration coefficient (in meter per hour) and h is water depth (in meter). K is calculated from the empirical equation developed by Thibodeaux et al. (1994) for the specific case of the Seine River:

$$K = \sqrt{\frac{D_\mathrm{m} \times V_\mathrm{wa}}{h}} + \left(k_\mathrm{wind} \times V_\mathrm{wi}^{2.23} \times D_\mathrm{m}^{\frac{2}{3}}\right)$$

where D_m is the molecular diffusivity of DO (in square meter per second), V_wa is the water velocity (in meter per second), k_wind is an empirical coefficient relating to wind aeration (3.3×10^{-4} m s^{-1}), and V_wi is the wind velocity (in meter per second).

For each time interval, the instantaneous DO rate of change corrected for F corresponds to the instantaneous DO net production rate, also called net primary production (NPP(t)) during light period. Instant Ecosystem Respiration (ER(t)) is calculated from average night time DO net production. ER(t) is assumed to be constant during the night and light periods, and daily ER is extrapolated from the instantaneous rates to 24 h. The instant gross primary production (GPP(t)) is computed as the sum of NPP(t) and ER(t) for each time interval and integrated during the light period to obtain daily GPP. The daily net ecosystem production (NEP) is calculated as the difference between daily rates of ER and GPP, and daily P/R as the ratio of GPP/ER. The volumetric estimates (in gram of O_2 per cubic meter per day) are converted to areal units (in gram of O_2 per

square meter per day) by multiplying by the effective water depth.

Conversions from carbon to oxygen are calculated assuming photosynthetic and respiratory quotients of 1.2 and 0.85, respectively (Bott et al. 2006).

Discrete sampling and analytical procedures

Grab water samples were collected every two weeks or monthly during field campaigns, in order to perform complementary analyses at the laboratory. These samples were integrated at the depth of sensor measurements, i.e., 1 m, using a Niskin bottle (KC-Denmark, Silkeborg, Denmark).

Samples collected for dissolved organic carbon (DOC) concentration measurements were filtered through pre-weighted and pre-combusted (525 °C) glass fiber filters (0.7 μm GF/F Whatman®, Maidstone, UK) and acidified with concentrated H_3PO_4 (85 %) in pre-cleaned and pre-combusted glass vials and then stored in the dark at 4 °C. After filtration, filters were dried at 105 °C and weighted to determine total suspended matter (TSM) content. After 12 h acidification under concentrated HCl acid vapor, each filter was cut in eight parts, four of which were weighted (±0.001 dry weight) and used for particulate organic carbon (POC) and particulate nitrogen (PN) concentration determination. Measurements were performed using a Thermo Scientific Flash 2000 organic elemental analyzer (Thermo Scientific, Waltham, MA, USA). DOC concentrations were measured with a Shimadzu TOC-VCSH analyzer (Shimadzu Corp., Kyoto, Kyoto Prefecture, Japan).

Samples collected for nutrients and alkalinity analyses were filtered on the field through 0.2-μm-pore size cellulose acetate filters (Sartorius Minisart, Sartorius AG, Goettingen, Germany) and stored at 4 °C in the dark. Nutrient concentrations (NO_3^-, NO_2^-, NH_4^+, SiO_2, and SRP) were determined by colorimetric titration using a Seal Quaatro Microflow analyzer (Seal Analytical, Hampshire, UK). Alkalinity was measured by the Gran method using an automated acid–base titrator (809 Titrando series, Metrohm, Herisau, Switzerland) with a precision of 1 %.

Chl*a* was extracted using neutralized methanol/water (90/10 *v*/*v*) by homogenization and resting for 16 h at 4 °C. Chl*a* concentrations were then measured using spectrophotometry according to Catherine et al. (2012). Samples for phytoplankton microscopic analyses were fixed in buffered formaldehyde (2 % *v*/*v* final concentration, pH 6.9; Merck, Darmstadt, Germany) and stored at 4 °C in the dark. Species identifications were performed using an Optiphot 2 light microscope and specific mean biovolumes were estimated from at least 30 individual measurements using a Digital Sight DS-L1 image acquisition system (Nikon Instruments Inc., Melville, NY, USA). Phytoplankton enumerations were realized according to Utermöhl method (1958), using an Eclipse TS100 inverted microscope (Nikon Instruments Inc.). Counts were then converted to biovolume by applying the mean biovolume determined for each species.

Data analyses

The DO and Chl*a* continuous time series were smoothed by a running average of one hour window to reduce estimate uncertainties in metabolism rates and productivity calculations (Staehr et al. 2010). Metabolic rates were also assessed at the seasonal scale. Therefore, seasons were delimited as periods of three months (i.e., winter (January–March), spring (April–June), summer (July–September) and autumn (October–December).

Some periods of malfunction of the CarboSeine station lead to a few gaps in the time series for the year 2011. During severe rain episodes, strong CSO water pulses yielded questionable estimates of metabolism rates, associated with rapid discharge increases and strong C_{25} variations. These observations did not comply with the single station hypothesis of water masses homogeneity (Needoba et al. 2012). Corresponding results were therefore excluded from the data analysis.

All statistical analyses were performed on $\log_{10}(x)$ transformed data, with the addition of a constant when needed, in order to increase variance stability and improve normality (Hunt et al. 2012). Variance analysis of the seasonal metabolic rates was performed using Kruskall–Wallis test and post hoc multiple comparison was carried out with Tukey's test. Multicollinearity of metabolism and independent variables (daily integrals of global light radiation (GLR), rainfall and CSO events, daily mean of *T*, Chl*a*, C_{25}, and turbidity) was tested using Pearson's correlation matrix. The correlation-based ordination of metabolism and independent variables was also assessed through principal components analyses (PCA) on standardized variables. The relationships between GPP or ER and independent variables, considered as important environmental regulators, were further investigated by pairwise linear regressions, using Sigmaplot© (2010 Systat Software Inc.).

Multiple linear regression analyses (MLR) were used to assess the combinations of independent variables that explain the highest variance in daily metabolism rates. A parsimony analysis was performed through the stepwise forward selection procedure to avoid spurious fit of models and explained variance inflation. MLR models were fitted to standardized independent variables to eliminate unit scale effects and determine which predictor had the largest effect on the response variable. MLR analyses were conducted with the "stepwisefit" function in Matlab environment (2012, The MathWorks, Inc.).

Results

Continuous hydrological and biogeochemical time series

Mean daily discharge of the Seine River at Bougival was characterized by a clear seasonal pattern with the highest baseflows of 300–350 $m^3\ s^{-1}$ range during winter, and the lowest baseflows (i.e., 75 $m^3\ s^{-1}$) in summer (Fig. 2a). These maximum and minimum discharge values correspond to water velocities of 1.02 and 0.21 m s^{-1}, respectively. Water *T* exhibited an inverse seasonal pattern with a minimum value of 5 °C observed during winter and a maximum value of 24 °C during late summer (Fig. 2a). This trend is mainly driven by GLR received in this part of the river, which is not shaded by forest canopy. Daily GLR maximum values (i.e., up to 8,000 W m^{-2}) were observed during summer, whereas minimum values (i.e., 110 W m^{-2}) occurred during cloudy winter days (Fig. 2b). Due to cloudy episodes, instantaneous GLR values displayed more variability than water *T*, whose variations are buffered by the large volume of the river. The year 2011 was quite dry compared to average precipitation statistics in Paris (i.e., 370 and 650 mm, respectively), and showed a bimodal pattern. The first half of the year was characterized by low rainfalls and the second half (June–December) exhibited large summer storm events, with maximum daily precipitations of 18 mm (Fig. 2b). These storm events may have been associated to CSO pulses to the river. Such CSO pulses can induce an increase of daily discharge up to two fold and severe C_{25} variations, as observed on the 19th of July during low flow periods (Fig. 2a).

Three main episodes of phytoplankton blooms, which were all composed of species from the "brown" spectral group, were recorded during 2011 (Fig. 2c). These episodes were characterized by maximum DO concentrations that were maintained above the saturation level (i.e., 130 %) during both dark and light periods. The first bloom was observed during late winter, mainly in March, reaching the maximum value of 55 μg Chl*a* L^{-1} during several days. The second bloom reached a lower maximum value (i.e., 20 μg Chl*a* L^{-1}) and was observed during spring, in May. This bloom was characterized by two main phases of Chl*a* increase and a transition period during which DO concentrations were below the saturation level. Finally, the third episode occurred during the first days of summer and led to the maximum value of 45 μg Chl*a* L^{-1}. These blooms showed distinct patterns of community compositions, according to biovolume measurements (see Electronic supplementary material (ESM) Fig. S1). The winter bloom was dominated by the diatoms species *Nitzschia spp.*, *Synedra ulna*, and *Cyclotella spp*. A different genus of diatoms (i.e., *Cyclotella spp*) dominated the summer bloom, during which it accounted for approximately 100 % of the total biovolume. Interestingly, the spring bloom was also composed of diatoms, but was dominated by the dinoflagellate *Peridinium sp.*, with respective contributions of 27 and 73 % to the total biovolume.

Water chemistry

Average total alkalinity and pH values were found to be 3,820 ± 326 μM (range, 3,330–4,321) and 7.89 ± 0.24 (range, 7.47–8.23), respectively, and displayed maximum values during winter (Table 1). TSM and POC concentrations were on average 16.9 ± 14.1 mg L^{-1} (range, 3.1–32.7) and 1.2 ± 0.6 mg L^{-1} (range, 0.5–2.1), respectively, with maximum values in autumn and winter, when discharge was high (Table 1 and Fig. 2a). Maximum values of the C/N ratio were measured concomitantly, whereas lower ratios were obtained in spring and summer, when high values of Chl*a* were registered. On average, DOC concentrations equaled 3.4 ± 1.1 mg L^{-1} (range, 2.2–6.7) and did not vary seasonally. Dissolved inorganic nitrogen, mainly present as NO_3^-, did not display any distinct seasonal pattern and its average concentration was 329 ± 81 μM (range, 192–462). Ammonium concentrations ranged from 3.3 to 17.2 μM, but often remained below a value of 10 μM (Table 1). SRP and SiO_2 concentrations averaged 1.9 ± 1.3 μM (range, <d.l.–4) and 113 ± 31.8 μM (range, 46.8–156), respectively, and exhibited minimum values during late winter and early spring, when Chl*a* concentrations were high. Interestingly, maximum values of SRP and NH_4^+ concentrations were measured on the 16th of June, after an important storm event characterized by daily precipitations of 18 mm.

Temporal patterns in river metabolism

Daily rates

Overall, 218 values of daily GPP, ER, NEP, and P/R rates were obtained from January to December 2011 (Fig. 3). The gaps corresponded to periods of malfunction of the station ($n = 64$) and to days, for which the metabolism quantification was not applicable (i.e., GPP < 0 and/or ER < 0, $n = 50$). Some questionable estimates, obtained during transient events, were also discarded from the data analysis ($n = 33$) due to the permanent state assumption.

According to the analytical solution of Reichert et al. (2009), and based on water velocities and K values (i.e., ranging from 0.037 to 0.078 m h^{-1}) at Bougival, the single station estimates were supposed to be influenced by processes occurring from 35 to 80 km upstream from the CarboSeine monitoring station. This corresponds to the distances separating Bougival from the previous station of Suresnes or the confluence between the Seine and Marne Rivers upstream from Paris, respectively (Fig. 1).

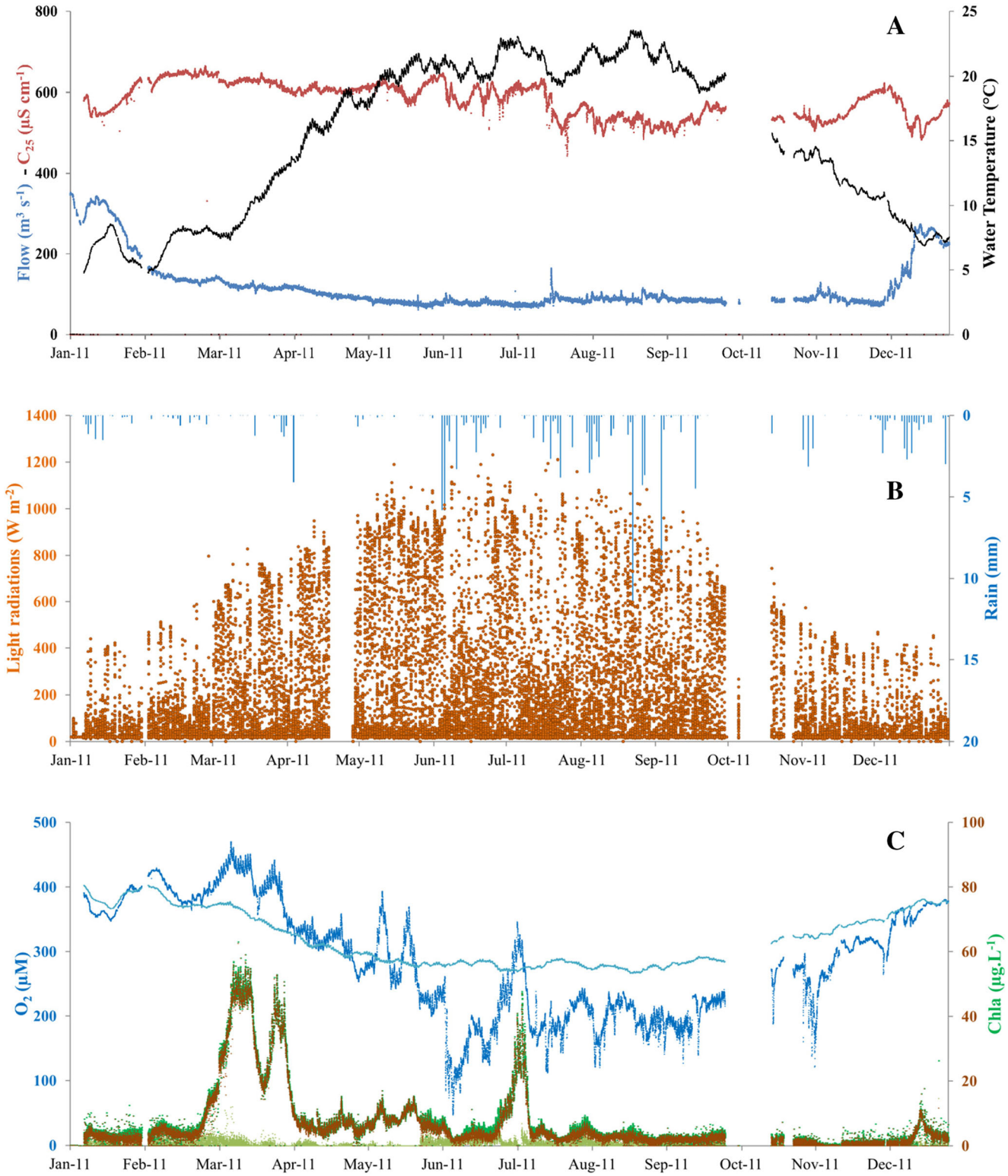

Fig. 2 CarboSeine's continuous hydrological and biogeochemical time series recorded at Bougival in 2011. **a**–**b** Parameters correspondence given by color code on respective *y*-axis. **c** DO measurements and theoretical DO saturation in *dark* and *light blue*, respectively. Total Chl*a* and relative contributions of "brown" and "green" spectral groups in *dark green*, *brown*, and *light green*, respectively

GPP and ER rates ranged from 0.04 to 15.7 and from 0.03 to 17.6 gO_2 m^{-2} day^{-1}, respectively. Their estimates largely mirrored each other throughout the year (Fig. 3a). Minimum rates of GPP and ER were observed during high flow periods (in autumn and winter). Maximum rates occurred from late winter to early summer during phytoplankton blooms.

Table 1 Mean (±1 SD) of Seine water chemistry analyses performed on grab samples

Date	Alkalinity (μM)	pH	TSM (mg L^{-1})	POC (mg L^{-1})	PN (mg L^{-1})	C/N ratio	Chl*a* (μg L^{-1})	DOC (mg L^{-1})	SiO_2 (μM)	SRP (μM)	NO_3^- (μM)	NH_4^+ (μM)	NO_2^- (μM)
January 6, 2011	4,245	8.20	32. 7	1.79 ± 0.05	0.28 ± 0.01	7.49	4.27 ± 0.17	–	131.6	a.d.l.	423.6	6.67	6.91
February 3, 2011	4,196	8.06	27.6	1.84 ± 0.03	0.25 ± 0.01	8.73	4.08 ± 0.04	2.89	139.0	2.14	426.1	4.44	3.52
March 3, 2011	4,322	8.20	19.1	1.59 ± 0.08	0.25 ± 0.01	7.53	20.48 ± 0.37	3.59	102.6	a.d.l.	462.2	6.67	2.95
March 24, 2011	4,130	8.23	11.6	1.32 ± 0.09	0.23 ± 0.01	6.61	29.78 ± 0.24	3.54	46.8	a.d.l.	411.3	3.33	3.11
April 13, 2011	4,014	–	12.2	0.80 ± 0.10	0.14 ± 0.01	6.45	8.71 ± 0.27	3.18	59. 9	a.d.l.	399.5	4.44	0.14
April 28, 2011	3,900	7.89	–	–	–	–	9.97 ± 0.37	–	64.6	1.00	343.0	9.44	3.24
May 26, 2011	3,618	7.66	8.3	0.89 ± 0.06	0.15 ± 0.01	6.90	7.46 ± 0.37	3.06	118.1	2.88	336.8	5.56	4.76
June 16, 2011	3,604	7.47	5.9	0.54 ± 0.00	0.11 ± 0.01	5.74	4.15 ± 0.20	3.12	156.7	4.00	298.6	15.00	5.07
July 7, 2011	3,804	7.97	3.8	1.18 ± 0.01	0.23 ± 0.01	5.93	34.99 ± 0.33	2.17	111. 9	2.20	232.5	3.33	3.01
July 27, 2011	3,367	7.62	17.5	0.93 ± 0.03	0.15 ± 0.01	7.15	5.03 ± 0.09	2.63	133.1	3.97	191.9	7.78	4.52
September 16, 2011	3,330	7.68	5.2	0.53 ± 0.05	0.10 ± 0.01	6.29	3.17 ± 0.14	6.72	132.5	2.26	255.8	17.22	4.67
October 5, 2011	3,506	7.70	9.9	0.77 ± 0.01	0.12 ± 0.01	7.31	2.95 ± 0.07	3.57	121.7	3.28	296.1	12.22	5.56
November 17, 2011	3,615	7.80	3.1	0.46 ± 0.02	0.08 ± 0.01	6.44	1.23 ± 0.58	2.68	129.4	2.29	258.9	5.00	4.63
December 14, 2011	3,599	7.98	26.0	2.11 ± 0.10	0.26 ± 0.01	9.57	2.70 ± 0.06	4.21	110.7	2.21	264.0	6.67	4.81

Although being characterized by strong day-to-day variability, these events coincided with periods of net autotrophy of the ecosystem (i.e., NEP > 0 and P/R > 1; Fig. 3b).

Seasonal rates

Rates of GPP and ER were, on average, higher ($p < 0.01$) during spring (4.8 ± 2.7 and 5.2 ± 2.9 $gO_2\ m^{-2}\ day^{-1}$, respectively) and summer (4.2 ± 3.4 and 5.9 ± 2.8 $gO_2\ m^{-2}\ day^{-1}$, respectively). Comparable maximum estimates were obtained during phytoplankton blooms in the spring and summer (Fig. 4a, b).

The relative magnitude of GPP and ER conditioned different typologies of net ecosystem production. Indeed, if the NEP rate gives information about the net C flux being processed throughout the ecosystem, the P/R ratio provides complementary insight on the trophic imbalance (Fig. 4c, d). On a seasonal basis, net autotrophy of the ecosystem was only observed during winter. Average P/R and NEP values reached 1.4 and 0.9 $gO_2\ m^{-2}\ day^{-1}$, respectively, and were mainly controlled by the phytoplankton bloom in March (Fig. 4c, d). Thus, even though the winter bloom was characterized by lower rates of GPP and ER compared to the spring and summer blooms, it was associated with a higher autotrophy of the ecosystem and maximum Chl*a* levels (Fig. 2). Maximum and minimum NEP rates (i.e., 7.27 and −6.16 $gO_2\ m^{-2}\ day^{-1}$) were observed during the onset of the spring bloom and the decline of the summer one (Fig. 3b), respectively. The corresponding seasonal average values of NEP and P/R indicated a progressive shift of the river metabolism towards heterotrophy all along the year (Fig. 4c, d). Spring NEP and P/R values (−0.4 ± 2.2 $gO_2\ m^{-2}\ day^{-1}$ and 1.0 ± 0.5, respectively) indicated quasi equilibrium between competing C production and consumption processes, whereas summer and autumn values suggested a dominance of respiration during the end of the year. Based on average P/R estimates, the ecosystem displayed higher heterotrophy in autumn, although minimum average NEP rates were observed during summer (Figs. 3b and 4c, d).

Annual estimates

At the annual scale, daily GPP and ER rates averaged 3.5 ± 2.9 and 4.1 ± 2.9 $gO_2\ m^{-2}\ day^{-1}$, respectively. As a result, average daily NEP rates (−0.6 ± 2.1 $gO_2\ m^{-2}\ day^{-1}$) indicated an annual net heterotrophy of the river ecosystem, associated with mean daily P/R ratio (0.9 ± 0.7) below the equilibrium threshold value (Fig. 4c, d).

Average daily metabolic rates were used to extrapolate annual rates. This approach yielded an annual GPP rate of 1,277 $gO_2\ m^{-2}\ year^{-1}$ or 399 $gC\ m^{-2}\ year^{-1}$, and an annual ER rate of 1,504 $gO_2\ m^{-2}\ year^{-1}$ or 663 $gC\ m^{-2}\ year^{-1}$. Overall, these calculations yielded an annual NEP rate of −226 $gO_2\ m^{-2}\ year^{-1}$ or −264 $gC\ m^{-2}\ year^{-1}$.

Drivers of river metabolism

GPP displayed significant correlations with all the independent variables considered (Table 2). More specifically, GPP was positively correlated with Chl*a* ($r = 0.57$), T ($r = 0.43$), and GLR ($r = 0.66$), and negatively correlated with rainfalls ($r = -0.23$) and CSO pulses ($r = -0.15$). ER was positively correlated with Chl*a* ($r = 0.16$), T ($r = 0.70$), and GLR ($r = 0.59$), but the correlation with Chl*a* was weaker than the one with GPP. NEP was significantly correlated with GPP and ER, with a higher correlation for the latter.

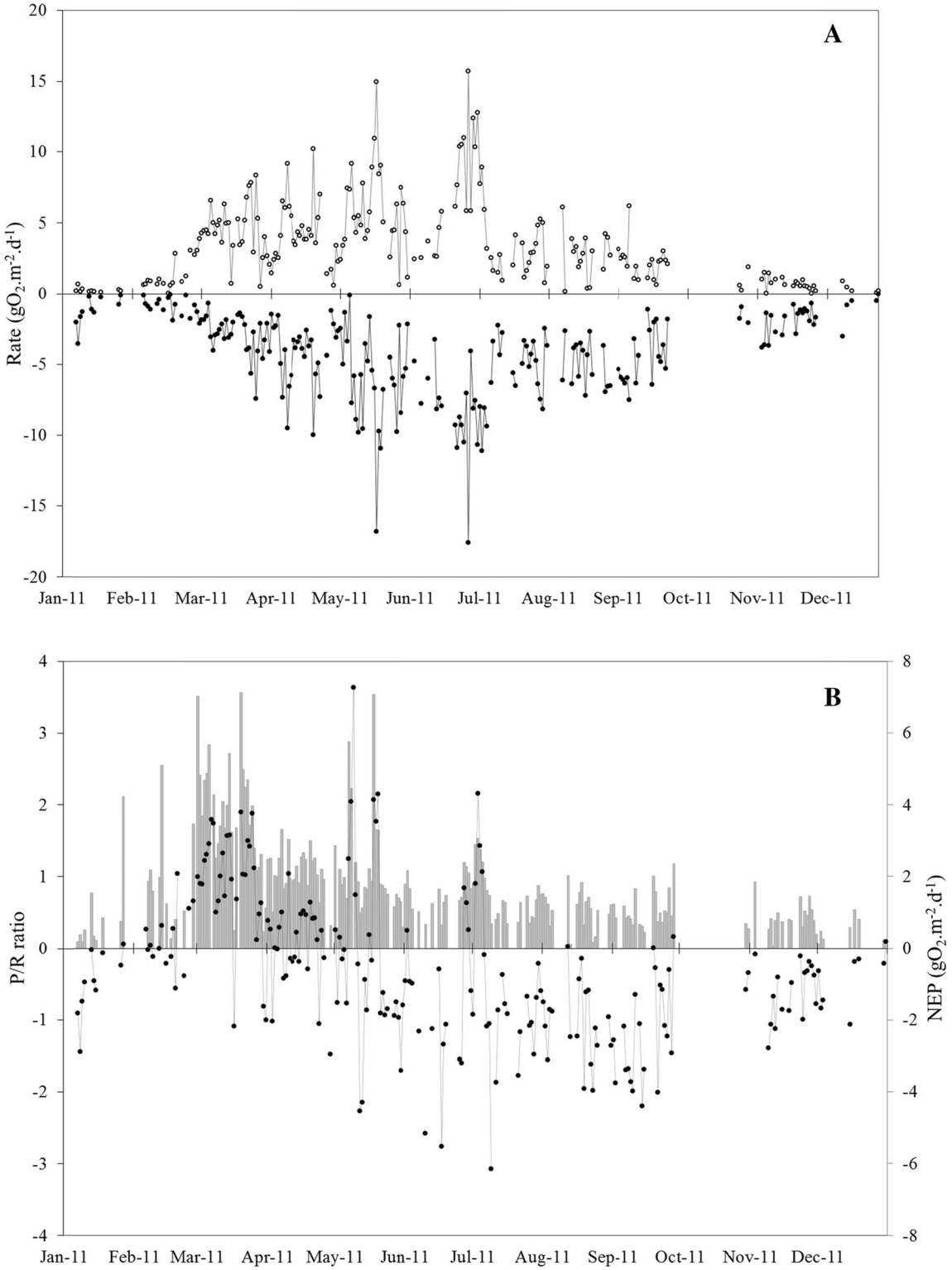

Fig. 3 Daily rates of (**a**) GPP (*grey line*), ER (negative values, *black line*), (**b**) NEP (*black circles*) and P/R ratio (*grey bars*) calculated at Bougival in 2011

Several independent variables displayed significant multicollinearity. This was also assessed through ordination on two principal components, which explained 61 % of the overall variance (see ESM Fig. S2). For instance, turbidity was significantly correlated with Chl*a* and GPP, but the correlations were partly biased by biofouling and confounding effects of phytoplankton cells on the sensor's optics.

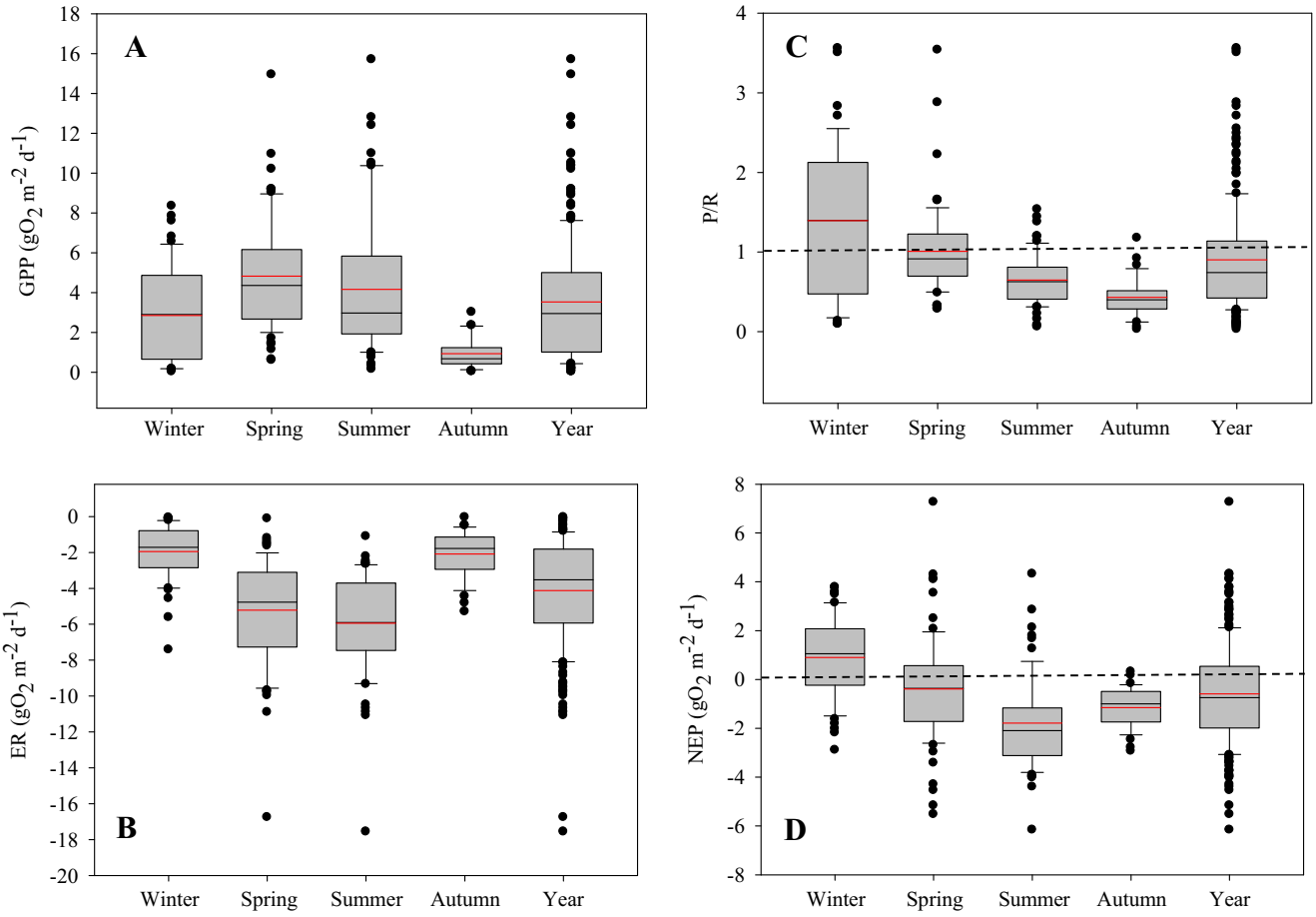

Fig. 4 Seasonal and annual variability of daily GPP (**a**), ER (**b**, as negative values), P/R (**c**), and NEP (**d**) rates ($n = 54$, 73, 63 and 28 days for winter, spring, summer, and autumn, respectively). *Bottom box lines* indicate the 25th percentile, *internal black* and *red lines* indicate median and mean values, respectively, and *top box lines* represent the 75th percentile. The *bottom* and *top whiskers* indicate the 10th and 90th percentile and *dots* indicate values that fall outside this range

The MLR analyses through stepwise forward selection resulted in a four-parameter model for GPP (Table 3) that explained nearly 62 % of the daily rates' variations by Chl*a*, *T*, GLR, and rainfalls. Based on standardized regression coefficients, Chl*a* was the most influential descriptor, accounting for 32 % of the variations in daily

Table 2 Pearson's correlation matrix on $\log_{10}(x)$ transformed daily metabolism rates and daily values of independent variables. Bold values indicate significant correlation (r, $p < 0.05$) among variables

	GPP	ER	NPP	NEP	Rain	Chl*a*	CSO	*T*° water	Turbidity	C_{25}	GLR
GPP	1.00										
ER	**0.72**	1.00									
NPP	**0.79**	**0.20**	1.00								
NEP	**0.30**	**−0.41**	**0.80**	1.00							
Rain	**−0.23**	−0.05	**−0.27**	**−0.21**	1.00						
Chl*a*	**0.57**	**0.16**	**0.63**	**0.48**	−0.08	1.00					
CSO	**−0.15**	−0.06	−0.13	−0.09	**0.70**	0.02	1.00				
T° water	**0.43**	**0.70**	−0.02	**−0.37**	−0.05	**−0.13**	**−0.18**	1.00			
Turbidity	**0.20**	−0.03	**0.33**	**0.30**	0.12	**0.48**	**0.18**	**−0.27**	1.00		
C_{25}	**0.27**	−0.13	**0.43**	**0.47**	−0.11	**0.62**	−0.05	**−0.31**	**0.23**	1.00	
GLR	**0.66**	**0.59**	**0.37**	0.04	**−0.28**	**0.32**	**−0.32**	**0.68**	0.00	0.06	1.00

Table 3 Multiple linear regression (MLR) model outputs for daily GPP ($p < 0.001$), ER ($p < 0.001$), and NEP ($p < 0.001$) as functions of daily values of independent variables

Dependent variable	Coefficient	MLR models Independent variable	β	p value	Cumulative adjusted R^2
$\log_{10}$(GPP)	0.217	$\log_{10}$(Chl*a*)	0.084	<0.001	0.322
	0.321	$\log_{10}$(T° water)	0.053	<0.001	0.581
	0.090	$\log_{10}$(GLR)	0.036	0.002	0.611
	−0.060	$\log_{10}$(rain)	−0.017	0.018	0.619
	−0.623				
$\log_{10}$(ER)	0.663	$\log_{10}$(T° water)	0.110	<0.001	0.489
	0.100	$\log_{10}$(Chl*a*)	0.038	<0.001	0.553
	−0.600				
$\log_{10}$(NEP)	0.052	$\log_{10}$(Chl*a*)	0.020	0.001	0.227
	−0.213	$\log_{10}$(T° water)	−0.035	<0.001	0.323
	−0.040	$\log_{10}$(rain)	−0.011	0.015	0.359
	0.041	$\log_{10}$(GLR)	0.017	0.025	0.372
	0.408	$\log_{10}$(C_{25})	0.012	0.032	0.382
	−0.605				

β = standardized partial regression coefficient

rates. Although GPP was better correlated with GLR than with T (Table 2), the MLR model suggested a higher influence of the latter (Table 3).

The MLR resulted in a two-parameter model for ER explaining 55 % of the variation in daily estimates by T and Chl*a* (Table 3). The former descriptor explained almost 49 % of the observed variance. The MLR model for ER displayed a lesser influence of Chl*a*, as compared with GPP. It is also worth noting that the MLR model did not include rainfall as a significant descriptor of daily ER rates variations, while it did for GPP (Table 3).

NEP was predicted by a five-parameter MLR model, containing the variables that significantly contribute to GPP and ER models, but also C_{25}. This model explained only 38 % of the variations in daily NEP rates, and Chl*a* was confirmed as the most influential descriptor, explaining around 23 % of the observed variance.

Productivity of phytoplankton communities

The control on river metabolism by phytoplankton was particularly noticeable during the three seasonal blooms, when DO and Chl*a* concentrations displayed related dynamics (Fig. 5a–c). At the daily scale, Chl*a* values were characterized by diel oscillations, nearly synchronized with the DO variations. The corresponding maximum Chl*a* amplitudes were mostly related to maximum Chl*a* levels, particularly for the late winter and summer blooms (Fig. 5a, c).

Based on the results of grab sample analyses (Table 1), concomitant FP measurements (as y, hereafter) consistently estimated cellular Chl*a* concentrations (as x, hereafter) determined by spectroscopic analysis ($y = 1.13x - 0.22$, $R^2 = 0.96$, $p < 0.001$). Thus, daily GPP rates were standardized by mean daily Chl*a* values, to assess the phytoplankton productivity rates associated with the different blooms (in gram of O_2 per gram of Chl*a* per day, Fig. 5d–f). Productivity rates ranged from 3 to 340 $gO_2\ gChla^{-1}\ day^{-1}$. Productivity rates were significantly higher ($p < 0.01$) during spring and summer blooms (i.e., 153 ± 61 and 169 ± 108 $gO_2\ gChla^{-1}\ day^{-1}$), compared to the winter ones (35 ± 15 $gO_2\ gChla^{-1}\ day^{-1}$), even though the spring bloom displayed lower Chl*a* levels (Fig. 5d–f). Each bloom was also characterized by an important day to day variability, with coefficients of variation of daily productivity rates ranging from 40 % during spring to 63 % during summer. Minimum rates were mostly associated with low GLR during cloudy days, as observed during the winter bloom (e.g., March 17, 2011 and March 30, 2011). The temporal pattern of daily productivity rates in March was significantly correlated with daily GLR values ($r = 0.79$, $p < 0.01$; $\log_{10}$ transformed values), while the relationship was not significant for the two other blooms.

Interestingly, additional SRP measurements, performed during the summer phytoplankton bloom, illustrated a concomitant significant decline in SRP concentrations and productivity rates ($r = 0.80$, $p < 0.01$; $\log_{10}$ transformed values), associated with an increase in Chl*a* (Figs. 5c, f and 6).

Discussion

The results presented in this study highlight the temporal dynamics of the metabolism of the highly anthropized Seine River and provide information about the associated environmental drivers. Based on multivariate analyses, several

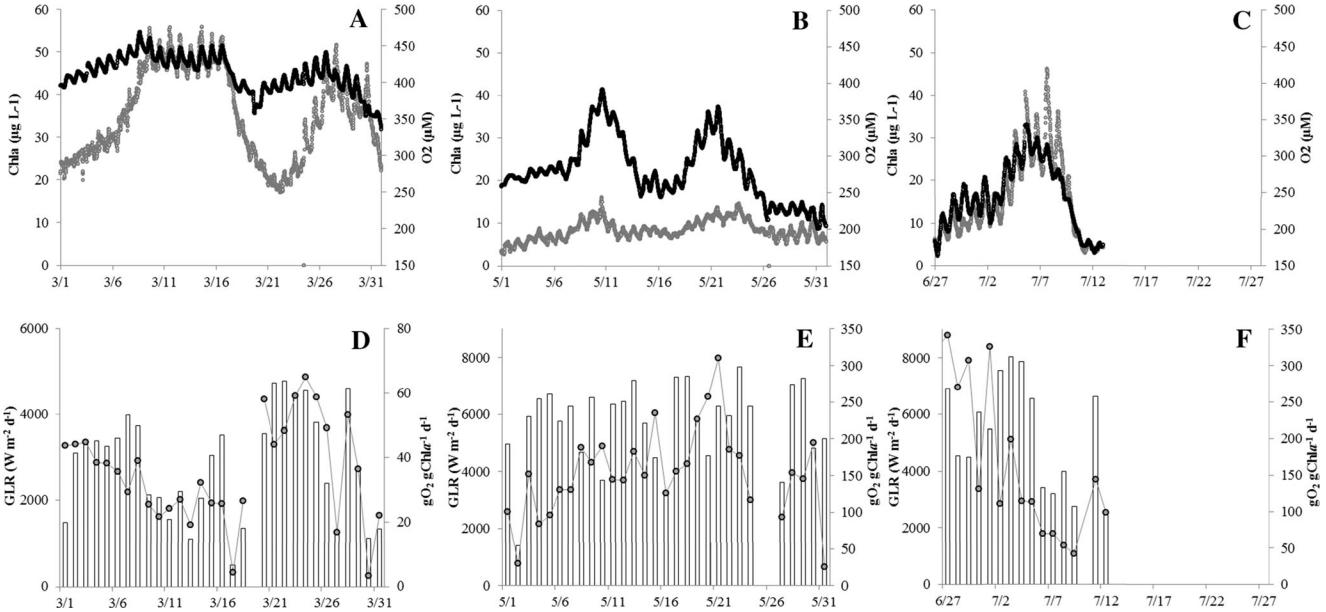

Fig. 5 **a**–**c** Continuous DO (*black line*) and Chl*a* (*grey line*) concentrations measured at Bougival during seasonal phytoplankton blooms. **d**–**f** Daily GLR (*white bars*) and productivity rates (*grey dots*) calculated from continuous measurements. Note different *y*-axis scales on **d**

controls of river metabolism are identified and exert variable influences, depending on the metabolic processes considered. These drivers act at various timescales, and lead to different typologies of net metabolism along the considered annual cycle.

Controls on GPP

Daily GPP rates are best described by a combination of Chl*a*, *T*, GLR, and rain, with Chl*a* being the most influential descriptor, just as for NEP rates (Table 3). The Seine river metabolism is, indeed, influenced by phytoplankton blooms, occurring from late winter to early summer (Figs. 2 and 3). Even though we did not investigate the potential contribution of the benthic component to GPP, the large depth of the river in the studied reach and the tight coupling between DO and Chl*a* time series (Figs. 2 and 5) likely suggest that GPP is pelagic rather than benthic. This result is in agreement with previous data obtained on the fourth-order Grand Morin stream, which is an affluent of the Seine River upstream from Paris area (Flipo et al. 2007). Regarding the metabolism of the dominant periphytic communities, Flipo et al. (2007) documented lower GPP and ER rates (three to six times, respectively), than those obtained in our study. However, they also evidenced that the net photosynthetic activity of the phytoplankton was higher than the one of the periphyton and that periphyton scouring was accounting for 7 % of the phytoplankton enrichment downstream. This is consistent with the predictions of the RCC regarding the dominance of pelagic processes in high order rivers. To our knowledge, the data presented in our study are the first documenting this control at such a resolution for a large human-impacted river. The relation between Chl*a* concentrations and GPP rates is however not straightforward. Maximum Chl*a* values are not related to maximum GPP rates, but rather coincide with the seasonal net autotrophy of the ecosystem (Fig. 4). This observation confirms the dependence of GPP upon other conditional drivers.

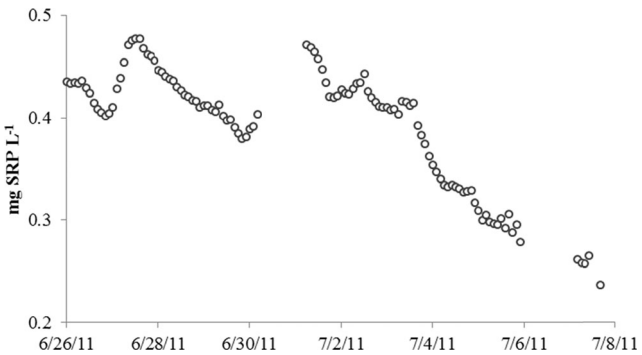

Fig. 6 High frequency (every 2 h) measurements of SRP concentrations at Bougival during summer phytoplankton bloom

Indeed, *T* and GLR are also identified as significant predictors of GPP (Table 3), and higher GPP rates are associated with maximum values of *T* and GLR in spring and summer (Figs. 2 and 3). Surprisingly, MLR analyses identify a higher influence of *T*, compared to GLR, although GPP is better correlated with the latter (Table 2). Several studies of stream metabolism have failed to detect such a direct effect of *T* (Roberts et al. 2007; Beaulieu et al. 2013), whereas it has been confirmed in other studies on large rivers (Uehlinger 2006;

Hunt et al. 2012). This may be explained by the different buffering capacities of the water volumes of these studied ecosystems. Moreover, considering large rivers, a stable progressive increase of *T* may enhance the photosynthetic activity at a seasonal scale (Townsend et al. 2011). GLR may exert a seasonal control on GPP through the length of the photoperiod. However, as observed during cloudy days in March (e.g., March 17, 2011; Fig. 5a), GLR can also have a significant influence at the daily scale, since it determines the amount of energy available for photosynthesis. A deterministic interpretation is difficult to provide with a statistical tool such as MLR, because *T* and GLR display collinearity in our dataset (Table 2). Such a limitation was already reported (Hunt et al. 2012). Beaulieu et al. (2013) using alternative methods (i.e., generalized least squares model), suggested a synergistic interaction of both parameters, with *T* that may enhance the capacity of autotrophs to use available light. Finally, rain precipitation is identified as the last driver of GPP (Table 3), with a negative influence, probably acting through the immediate reduction of received GLR (e.g., March 30, 2011; Fig. 5a) and the potential dilution effect of river water (Even et al. 2004).

Overall, albeit being highly significant ($p < 0.001$), the MLR model obtained for GPP is also characterized by a relatively important unexplained variance (Table 3). In this sense, further analyses of the CarboSeine's continuous measurements and discrete field data provide complementary information. Discharge is not investigated as a controlling factor, due to its use for the back calculation of water velocities, which are used for the estimation of the reaeration and metabolic rates. It is, however, very likely that the decrease in discharge and TSM concentrations after February (Fig. 2 and Table 1) has favored phytoplankton growth by increasing light availability within the water column. This cannot be confirmed by turbidity measurements, because of the sensor's malfunction at this time. Yet, this control of discharge and TSM on GPP has already been emphasized for the Seine River (Garnier et al. 1995) and other lotic systems (Acuna et al. 2004; Izagirre et al. 2008).

The composition of phytoplankton communities and the associated productivity rates constitute another important piece of information. The FP used in this study is specifically calibrated with diatoms species of the Seine River that belong to the "brown" spectral group (Escoffier et al. 2015). Based on this specific SFS, the FP measurements are consistent with the cellular Chl*a* concentrations determined with the spectroscopic reference method. Therefore, the estimated productivity rates are in the close range of those estimated by Oliver and Merrick (2006) regarding the contribution of pelagic diatoms to the metabolism of the seventh-order Murray River in Australia. Considering the spring and summer blooms, our estimates are, however, slightly higher than their reported values (i.e., 2–180 $gO_2\,gChla^{-1}\,day^{-1}$). This may originate from the composition of communities. Indeed, the specific SFS used does not allow for the differentiation between the diatom and dinoflagellate species constituting the winter/summer and spring communities, respectively (ESM Fig. S1), and interspecific differences in photosynthetic capacities have long been recognized (Falkowski and Raven 2007). However, other factors may also induce confounding effects.

The role of nutrient concentrations in controlling metabolic performances must particularly be considered. Due to agricultural practices on the watershed and the urban influence of the Paris conurbation, the Seine River displays a eutrophic status associated with high concentrations of N and P (Garnier and Billen 2007). Despite not being completely recorded by continuous measurements, the temporal pattern of nutrient concentrations (partly described through discrete sampling) presents complementary insights. The winter bloom is mainly composed of pennate diatoms. Although productivity rates are correlated with GLR (Fig. 4d), depleted concentrations of SiO_2 and particularly SRP are noticed in March (Table 1). This seasonal depletion of SiO_2 following the winter development of diatoms has already been reported in the Seine River (Garnier et al. 1995). It likely explains the succession towards the dominance of dinoflagellates, observed during the spring blooms. The spring and summer productivity rates of phytoplankton are, on the contrary, not significantly correlated with GLR (Fig. 5e, f). Considering the summer bloom, productivity rates are significantly correlated with average daily SRP concentrations calculated from continuous measurements ($r = 0.80$, $p < 0.01$, Fig. 6). This result suggests a significant uptake of SRP by phytoplankton, as previously reported (Roberts et al. 2007; Bernot et al. 2010). Using a C/Chl*a* ratio of 30 (Flipo et al. 2007), during the period of Chl*a* increase and SRP decrease in early July, we estimate a C/P molar ratio of 63, which is lower than the theoretical Redfield ratio (i.e., 116). Therefore, the growth of phytoplankton is likely not limited by P-availability, even though the enhanced diel Chl*a* fluorescence oscillations observed at the end of the bloom may characterize nutrient limitation (Kruskopf and Flynn 2007; Escoffier et al. 2015).

Controls on ER

Regarding the MLR model results, ER is best described by a combination of Chl*a* and *T* (Table 3). Chl*a* accounts for a relatively small amount of ER variance, and the correlation between daily Chl*a* values and ER rates is also lower than with GPP (Tables 2 and 3). This observation may be explained by the fact that the ER rates estimated from the used open water method do not allow the relative estimation of autotrophic and heterotrophic respirations (AR and HR, respectively; Hall and Beaulieu 2013).

Indeed, GPP is not included in the MLR model given the use of ER light rates for its calculation. GPP and ER rates are however strongly correlated (Table 2) and their maximum

estimates co-occur during phytoplankton blooms in the first part of the year. At these periods, it is therefore very likely that GPP, and most specifically AR, is contributing significantly to ER. For instance, Beaulieu et al (2013) estimated that around 70 % of newly fixed carbon was respired by autotrophs and closely associated heterotrophs in a low order urban stream. In the case of the Seine River, a recent modeling approach that allows for the distinction between the different respiration components (Vilmin et al. 2016) indicate that, in periods of low flow that coincide with periods of high productivity (P/R = 0.9), AR accounts for 19 % of ER. During high-flow periods (P/R = 0.3), even though the primary producer biomass is limited, its respiration still accounts for 15 % of ER.

Nevertheless, T is shown to be the main descriptor of ER, explaining 49 % of the observed variance (Table 3). ER is also significantly correlated ($p < 0.001$) with GLR but the MLR model sorts out the cross-correlation between T and GLR (Table 2) and shows that T has a greater effect. Such a control of temperature on respiration and photosynthesis is predicted by metabolic theory (Brown et al. 2004) and has been previously verified in other large river metabolism studies (Hunt et al. 2012; Dodds et al. 2013). A recent study using meta-analysis also demonstrates a similar sensitivity of ER to seasonal variations in temperature across terrestrial and aquatic ecosystems and confirms that this dependence propagates from the cellular to the ecosystem level in flowing waters (Yvon-Durocher et al. 2012). This control, however, is not systematically confirmed in whole ecosystem studies, since ER is also dependent on significant organic matter inputs that do not necessarily coincide with higher temperatures.

With regard to the Seine River, it must be underlined that both rain precipitation and CSO events are not correlated with ER and, therefore, they are not included in the MLR model (Tables 2 and 3). This may be related to the time lag between rain events and potential consecutive CSO pulses into the river, and also questions the reliability of MLR models to describe non-linear or non-instantaneous processes. Moreover, even though these events are clearly impacting DO concentrations (Fig. 2b, c), most of the corresponding days are eliminated from the dataset. Therefore, this prevents to assess the corresponding anthropogenic impact on river metabolism at the daily scale.

Nevertheless, the influence of rainfalls and CSOs is implied at the seasonal scale through the enhancement of ER rates and net heterotrophy of the river (i.e., NEP < 0 and P/R < 1, Figs. 3 and 4) from June to December 2011, when storm events are more frequent and associated with warmer temperatures (Fig. 2). During these periods of low discharge, CSOs represent the main allochtonous supply to the river and can induce a twofold increase of the river discharge (e.g., 19th of July; Fig. 2). According to previous investigations involving discrete sampling and modeling approaches, these CSO pulses deliver large inputs of POC, DOC, heterotrophic bacteria, and nutrients to the river that may stimulate respiratory processes in different ways (Servais et al. 1999; Even et al. 2004). The method used in our study does not allow partitioning the contributions of pelagic and benthic components but, at low flow, benthic respiration may account for one third of the overall respiration of the river (Vilmin et al. 2016). Due to rapid settling and low hydrolysis rates, discharged POC may have an indirect impact on oxygen deficit and may induce a delayed benthic oxygen demand, which depends on deposition–erosion processes occurring at low flow (Vilmin et al. 2015). Also, the discharge of highly labile DOC (up to 40 % of total DOC concentrations of CSO pulses, Even et al. 2004) and heterotrophic bacteria may enhance directly both pelagic and benthic respiration (Vilmin et al. 2016) and, as a consequence, the observed net heterotrophy in summer (Fig. 4). Several studies have confirmed this link between microbial respiration and DOC availability in flowing waters, especially in the context of human-dominated landscapes (Stanley et al. 2012). However, this control is not evident in our results given the low variability displayed by the DOC concentrations measured on discrete samples (Table 1). Inversely, grab sample analyses describe increased concentrations of SRP and DIN after the important storm event and associated CSO on the 5th June (Fig. 2b, c and Table 1). This nutrient enrichment is likely to enhance heterotrophic activity during the second half of the year through processes such as denitrification. At shorter time scales, it may also likely promote the phytoplankton bloom observed in July (Figs. 2 and 5). However, even though photosynthesis represents an important counter balancing factor for Seine River's oxygenation, the release of DOC and the settling of phytoplankton dead cells at the end of algal blooms may also constitute an additional organic supply for bacterial activity brought by the sewer system (Even et al. 2007).

Comparison with other lotic ecosystems

The continuous measurements of the CarboSeine station highlight the dynamics of the interplay between phytoplankton ecology, urban pressures and ecosystem functions at short timescales. At longer timescales they, additionally, allow for the calculation of annual estimates which are scarce for large river metabolism. These estimates are extrapolated from the calculated 218 daily rates and provide a consistent overview of the functioning of the ecosystem over an annual cycle.

These estimates also depend on an accurate parameterization of the diffusive exchange of O_2 with the atmosphere, which is a critical point in metabolism studies (Aristegi et al. 2009). As performed for other large rivers (Dodds et al. 2013; Demars et al. 2015), we use an empirical formula that was specifically developed for the Seine River (Thibodeaux et al. 1994). The range of estimated reaeration coefficients (i.e., 0.037 to 0.078 m h^{-1}) is consistent with estimates obtained

from reach-scale budgets in the downstream part of the Seine River (Garnier et al. 2001) and is representative of the values reported for large slow-moving waters (Maynard et al. 2012).

Annual estimates describe an overall net heterotrophy of the Seine River (NEP = −226 $gO_2\ m^{-2}\ year^{-1}$ or −264 $gC\ m^{-2}\ year^{-1}$) within the study area (Fig. 4). This result reinforces the common assumption of overall prevalence of net heterotrophy for inland waters (Duarte and Prairie 2005), even though it may be associated with varying magnitudes of GPP and ER rates. Based on average daily GPP and ER rates calculated for 2011, our results (1.10 ± 0.92 and 1.82 ± 1.31 $gC\ m^{-2}\ day^{-1}$, respectively) are comparable, although slightly higher for GPP, with the average conservative estimates published by Battin et al. (2008) for rivers. More specifically, our estimates are higher than rates in low nutrient streams and rivers in the tropics (Townsend et al. 2011; Hunt et al. 2012) or higher latitudes (Mulholland et al. 2001; Vink et al. 2005) and similar to rates reported for nutrient-enriched temperate streams (Bott et al. 2006). Expressed in terms of annual rates, our GPP and ER estimates (399 and 663 $gC\ m^{-2}\ year^{-1}$, respectively) fall again in the upper range of the few estimates available for rivers and recently synthesized by Dodds et al. (2013); (GPP range [50–356] $gC\ m^{-2}\ year^{-1}$, ER [73–588] $gC\ m^{-2}\ year^{-1}$, NEP [−588–90] $gC\ m^{-2}\ year^{-1}$).

These differences may, in part, be explained by the different methodologies used (e.g., continuous/discrete samplings, chambers/open-water techniques) and by the representativeness of the corresponding datasets. In our study, annual estimates are extrapolated from about 60 % of the days of the annual cycle. From a temporal perspective, most of the excluded days are grouped during autumn when the river is net heterotrophic and characterized by lower seasonal rates of GPP and ER. Another part of these days also correspond to summer storms and transient CSO events that violate the permanent state assumption. Therefore, it is likely that our approach may have slightly overestimated GPP rates and underestimated the net heterotrophy of the ecosystem. This statement confirms the necessity of acquiring nearly complete continuous time series to yield accurate estimates. According to the few references available for continuous monitoring of metabolism over annual cycles, our estimates are similar to rates reported for human-impacted streams or rivers (Uehlinger 2006; Izagirre et al. 2008; Beaulieu et al. 2013) and slightly higher than estimates obtained in a forested headwater stream (Roberts et al. 2007).

Besides these uncertainties in annual estimates, the high GPP and ER rates that are documented in this study may also reflect the influence of human pressures on the Seine River. Finlay (2011) investigated functional responses of lotic systems to resource enrichment at annual scales and demonstrated increased metabolic rates in streams, whereas this effect was not significant regarding rivers. Therefore, even though further work is required to investigate this impact in rivers with large watershed areas, it is most likely that nutrient enrichment from agricultural practices and waste water treatments (Garnier and Billen 2007) is enhancing the metabolism of the Seine River. N-pollution, in particular, is likely to increase GPP rates by favoring phytoplankton growth during stable discharge periods. On the other hand, N pollution stimulates the heterotrophic activity and associated ER rates through processes such as denitrification (Raimonet et al. 2015).

Regarding the present results, further work is required to assess their representativeness of the metabolism of the Seine River. Our estimates are in agreement with those previously obtained in reach-scale and modeling studies of the Seine River (Garnier et al. 2001; Garnier and Billen 2007; Vilmin et al. 2016), which also document a strong longitudinal variability of biogeochemical processes from Paris to the entrance of the estuary. These spatial heterogeneities are notably related to different WWTP influences (Vilmin et al. 2016) and they must be accounted for in order to better understand the control that anthropogenic and environmental drivers exert on river metabolism. For instance, CSOs impact has not been directly evidenced at the daily scale but still its influence is perceptible at the longer timescales. Despite improvements in wastewater treatments and land use exploitation, the Seine River remains eutrophicated and displays patterns of the "urban stream syndrome" (e.g., high-nutrient regimes, regulation of discharge, and input of episodic storm outflows). Thus, continuous monitoring of the Seine River metabolism at larger spatial and temporal scales should help to deepen our knowledge on the relative impacts of these controls. Furthermore, it should improve our understanding of the relationship between this functional indicator and structural metrics of water quality, as previously highlighted in rivers (Garnier and Billen 2007; Uehlinger 2006).

Conclusions

In this study, we were able to estimate the Seine River ecosystem metabolism over an annual cycle from continuous multi-sensor measurements. Our results provided evidence that as for most inland waters, the river was net heterotrophic at the annual scale. This implies that respiratory organic matter consumption exceeds photosynthetic production and thus assigns to flowing waters an important role to the lateral exchange of carbon between ecosystems. However, our estimates also confirmed that autotrophy may dominate over seasonal time scales. Even though they were consistent with those found for other type of rivers, they exhibited relatively high rates of GPP. The tight coupling between Chl*a* and DO confirmed that GPP was mainly pelagic, as suggested by the RCC, and related to the river phytoplankton blooms.

Temperature was shown to have a strong control on both GPP and ER while storm events were suspected to exert a control on ER at the seasonal scale through inflows of organic matter and nutrients released by CSOs. These inflows most probably have stimulated ER in both the water column and the benthic layer, even though the method used did not allow partitioning the roles of these two compartments. Coupled to less favorable conditions for photosynthetic production during the second half of the year, these human pressures enhanced the net heterotrophy of the river. Continuous monitoring proved to be a promising tool to improve our knowledge of the processes driving river metabolism at different time scales. Such an approach should, therefore, be maintained in the long term and extended in terms of spatial resolution, in order to consider this type of results in the context of changing human pressures and climate.

Acknowledgments This work was funded by the R2DS 2010 CarboSeine and PIREN-Seine research programs and also supported by a CIFRE grant awarded to N. Escoffier with Nke Instrumentation. L. Vilmin also benefited from a PhD fellowship funded by the Ile-de-France R2DS CarboSeine project. Most of the authors belong to the FR3020 FIRE (Fédération Ile-de-France de Recherche en Environnement). The authors thank the colleagues of the UMR 7245, Equipe CCE of the National Museum of Natural History for providing help on fluorometer calibration and phytoplankton analyses. The authors are also grateful to two reviewers for their useful comments.

Compliance with ethical standards

Conflict of interest The authors declare that they have no competing interests.

References

Acuna V, Giorgi A, Munoz I, Uehlinger U, Sabater S (2004) Flow extremes and benthic organic matter shape the metabolism of a headwater Mediterranean stream. Freshwater Biol 49:960–971

Aristegi L, Izagirre O, Elosegi A (2009) Comparison of several methods to calculate reaeration in streams, and their effects on estimation of metabolism. Hydrobiologia 635:113–124

Aufdenkampe A, Mayorga KE, Raymond PA, Melack JM, Doney SC, Alin SR, Aalto RE, Yoo K (2011) Riverine coupling of biogeochemical cycles between land, oceans, and atmosphere. Front Ecol Environ 9:53–60

Battin TJ, Kaplan LA, Findlay S, Hopkinson CS, Marti E, Packman AI, Newbold JD, Sabater F (2008) Biophysical controls on organic carbon fluxes in fluvial networks. Nat Geosci 1:95–100

Battin TJ, Luyssaert S, Kaplan LA, Aufdenkampe AK, Richter A, Tranvik LJ (2009) The boundless carbon cycle. Nat Geosci 2:598–600

Beaulieu JJ, Arango CP, Balz DA, Shuster WD (2013) Continuous monitoring reveals multiple controls on ecosystem metabolism in a suburban stream. Freshwater Biol 58:918–937

Benson BB, Krause JD (1984) The concentration and isotopic fractionation of oxygen dissolved in freshwater and seawater in equilibrium with the atmosphere. Limnol Oceanogr 29(3):620–632

Bernot MJ, Sobota DJ, Hall RO, Mulholland PJ, Dodds WK, Webster JR, Tank JL, Ashkenas LR, Cooper LW, Dahm CN, Gregory SV, Grimm NB, Hamilton SK, Johnson SL, McDowell WH, Meyer JL, Peterson B, Poole GC, Valett HM, Arango C, Beaulieu JJ, Burgin AJ, Crenshaw C, Helton AM, Johnson L, Merriam J, Niederlehner BR, O'Brien JM, Potter JD, Sheibley RW, Thomas SM, Wilson K (2010) Inter-regional comparison of land-use effects on stream metabolism. Freshwater Biol 55:1874–1890

Bott TL, Montgomery DS, Newbold JD, Arscott DB, Dow CL, Aufdenkampe AK, Jackson JK, Kaplan LA (2006) Ecosystem metabolism in streams of the Catskill Mountains (Delaware and Hudson River watersheds) and Lower Hudson Valley. J N Am Benthol Soc 25:1018–1044

Brown JH, Gillooly JF, Allen AP, Savage VM, West GB (2004) Toward a metabolic theory of ecology. Ecology 85:1771–1789

Catherine A, Escoffier N, Belhocine A, Nasri AB, Hamlaoui S, Yepremian C, Bernard C, Troussellier M (2012) On the use of the FluoroProbe (R), a phytoplankton quantification method based on fluorescence excitation spectra for large-scale surveys of lakes and reservoirs. Water Res 46:1771–1784

Cox BA (2003) A review of dissolved oxygen modelling techniques for lowland rivers. Sci Total Environ 314–316:303–334

Demars BOL, Thompson J, Russell Manson J (2015) Stream metabolism and the open diel oxygen method: Principles, practice, and perspectives. Limnol Oceanogr-Meth 13:356–374

Dodds WK, Cole JJ (2007) Expanding the concept of trophic state in aquatic ecosystems: It's not just the autotrophs. Aquat Sci 69:427–439

Dodds WK, Veach AM, Ruffing CM, Larson DM, Fischer JL, Costigan KH (2013) Abiotic controls and temporal variability of river metabolism: multiyear analyses of Mississippi and Chattahoochee River data. Freshwater Science 32:1073–1087

Duarte CM, Prairie YT (2005) Prevalence of heterotrophy and atmospheric CO_2 emissions from aquatic ecosystems. Ecosystems 8:862–870

EC (2000) European Commission Directive 2000/60/EC of the European Parliament and of the council of 23 October 2000 establishing a framework for Community action in the field of water policy. Off J Eur Commun L327:1–72

Escoffier N, Bernard C, Hamlaoui S, Groleau A, Catherine A (2015) Quantifying phytoplankton communities using spectral fluorescence: the effects of species composition and physiological state. J Plankton Res 37(1):233–247

Even S, Poulin M, Mouchel JM, Seidl M, Servais P (2004) Modelling oxygen deficits in the Seine River downstream of combined sewer overflows. Ecol Model 173:177–196

Even S, Mouchel M, Servais P, Flipo N, Poulin M, Blanc S, Chabanel M, Paffoni C (2007) Modelling the impacts of combined sewer overflows on the river Seine water quality. Sci Total Environ 375:140–151

Falkowski PG, Raven JA (2007) Aquatic photosynthesis, second edition. Princeton University Press, Princeton, New Jersey, p 484

Finlay JC (2011) Stream size and human influences on ecosystem production in river networks. Ecosphere 2(8):art87

Flipo N, Rabouille C, Poulin M, Even S, Tusseau-Vuillemin MH, Lalande M (2007) Primary production in headwater streams of the Seine basin: the Grand Morin river case study. Sci Total Environ 375:98–109

Garnier J, Billen G (2007) Production vs. respiration in river systems: An indicator of an "ecological status". Sci Total Environ 375:110–124

Garnier J, Billen G, Coste M (1995) Seasonal succession of diatoms and chlorophyceae in the drainage network of the seine river—observations and modeling. Limnol Oceanogr 40:750–765

Garnier J, Servais P, Billen G, Akopian M, Brion N (2001) Lower Seine river and estuary (France) carbon and oxygen budgets during low flow. Estuaries 24:964–976

Hall RO, Beaulieu JJ (2013) Estimating autotrophic respiration in streams using daily metabolism data. Freshwater Science 32(2):507–516

Hall RO, Tank JL (2005) Correcting whole-stream estimates of metabolism for groundwater input. Limnol Oceanogr-Meth 3:222–229

Hall RO, Tank JL, Baker MA, Rosi-Marshall EJ, Hotchkiss er (2015) Metabolism, gas exchange and carbon spiraling in Rivers. Ecosystems DOI: 10.1007/s10021-015-9918-1

Holtgrieve GW, Schindler DE, Branch TA, A'Mar ZT (2010) Simultaneous quantification of aquatic ecosystem metabolism and reaeration using a Bayesian statistical model of oxygen dynamics. Limnol Oceanogr 55: 1047–1063

Hunt RJ, Jardine TD, Hamilton SK, Bunn SE (2012) Temporal and spatial variation in ecosystem metabolism and food web carbon transfer in a wet-dry tropical river. Freshwater Biol 57:435–450

Izagirre O, Agirre U, Bermejo M, Pozo J, Elosegi A (2008) Environmental controls of whole-stream metabolism identified from continuous monitoring of Basque streams. J N Am Benthol Soc 27:252–268

Kruskopf M, Flynn KJ (2007) Chlorophyll content and fluorescence responses cannot be used to gauge reliably phytoplankton biomass, nutrient status or growth rate. New Phytol 169:525–536

MATLAB (2012) Version 8.0. The MathWorks Inc., Natick, Massachusetts

Maynard JJ, Dahlgren RA, O'Geen AT (2012) Quantifying spatial variability and biogeochemical controls of ecosystem metabolism in a eutrophic flow-through wetland. Ecol Eng 47:221–236

Millenium Ecosystem Assessment (2005) Ecosystems and human well-being: health synthesis., 64pp, WHO Library

Mulholland PJ, Fellows CS, Tank JL, Grimm NB, Webster JR, Hamilton SK, Marti E, Ashkenas L, Bowden WB, Dodds WK, McDowell WH, Paul MJ, Peterson BJ (2001) Inter-biome comparison of factors controlling stream metabolism. Freshwater Biol 46:1503–1517

Needoba JA, Peterson TD, Johnson KS (2012) Method for the Quantification of Aquatic Primary Production and Net Ecosystem Metabolism using in situ Dissolved Oxygen Sensors. *in* Molecular Biological Technologies for Ocean Sensing. Springer Protocols Handbooks, Chapter 4, pp 73–101

Odum HT (1956) Primary production in flowing waters. Limnol Oceanogr 1:102–117

Oliver RL, Merrick CJ (2006) Partitioning of river metabolism identifies phytoplankton as a major contributor in the regulated Murray River (Australia). Freshwater Biol 51:1131–1148

Raimonet M, Vilmin L, Flipo N, Rocher V, Laverman A (2015) Modeling the fate of nitrite in an urbanized river using experimentally obtained nitrifier growth parameters. Water Res 73:373–387

Raymond PA, Hartmann J, Lauerwald R, Sobek S, McDonald C, Hoover M, Butman D, Striegl R, Mayorga E, Humborg C, Kortelainen P, Dürr H, Meybeck M, Ciais P, Guth P (2013) Global carbon dioxide emissions from inland waters. Nature 503:355–359

Reichert P, Uehlinger U, Acuna V (2009) Estimating stream metabolism from oxygen concentrations: effect of spatial heterogeneity. Journal of Geophysical Research-Biogeosciences 114

Riley AJ, Dodds WK (2013) Whole-stream metabolism: strategies for measuring and modeling diel trends of dissolved oxygen. Freshwater Science 32:56–69

Roberts BJ, Mulholland PJ, Hill WR (2007) Multiple scales of temporal variability in ecosystem metabolism rates: results from 2 years of continuous monitoring in a forested headwater stream. Ecosystems 10:588–606

Servais PJ, Garnier J, Demarteau N, Brion N, Billen G (1999) Supply of organic matter and bacteria to aquatic ecosystems through wastewater effluents. Water Res 33:3521–3531

Staehr PA, Bade D, Van de Bogert MC, Koch GR, Williamson C, Hanson P, Cole JJ, Kratz T (2010) Lake metabolism and the diel oxygen technique: state of the science. Limnol Oceanogr-Meth 8:628–644

Stanley EH, Powers SM, Lottig NR, Buffam I, Crawford JT (2012) Contemporary changes in DOC human-dominated rivers: is there a role for DOC management? Freshwater Biol 57(Suppl 1):26–42

Strahler AN (1957) Quantitative analysis of watershed geomorphology. Transactions American Geophysical Union 38:913–920

Thibodeaux L, Poulin M, Even S (1994) A model for enhanced aeration of streams by motor vessels with application to the Seine river. J Hazard Mater 37:459–473

Townsend SA, Webster IT, Schult JH (2011) Metabolism in a groundwater-fed river system in the Australian wet/dry tropics: tight coupling of photosynthesis and respiration. J N Am Benthol Soc 30(3):603–620

Tranvik LJ, Downing JA, Cotner JB, Loiselle SA, Striegl RG, Ballatore TJ, Dillon P, Finlay K, Fortino K, Knoll LB, Kortelainen PL, Kutser T, Larsen S, Laurion I, Leech DM, McCallister SL, McKnight DM, Melack JM, Overholt E, Porter JA, Prairie Y, Renwick WH, Roland F, Sherman BS, Schindler DW, Sobek S, Tremblay A, Vanni MJ, Verschoor AM, von Wachenfeldt E, Weyhenmeyer GA (2009) Lakes and reservoirs as regulators of carbon cycling and climate. Limnol Oceanogr 54:2298–2314

Uehlinger U (2006) Annual cycle and inter-annual variability of gross primary production and ecosystem respiration in a floodprone river during a 15-year period. Freshwater Biol 51:938–950

Vannote RL, Minshall GW, Cummins KW, Sedell JR, Cushing CE (1980) River continuum concept. Can J Fish Aquat Sci 37:130–137

Vighi M, Finizio A, Villa S (2006) The evolution of the environmental quality concept: From the US EPA red book to the European Water Framework Directive. Environ Sci Pollut R 13:9–14

Vilmin L, Flipo N, Escoffier N, Rocher V, Groleau A (2016) Carbon fate in a large temperate human-impacted river system: focus on benthic dynamics. Global Biogeochem Cycles

Vilmin L, Flipo N, de Fouquet C, Poulin M (2015) Pluri-annual sediment budget in a navigated river system: the Seine River (France). Sci Total Environ 502:48–59

Vink S, Bormans M, Ford PW, Grigg NJ (2005) Quantifying ecosystem metabolism in the middle reaches of Murrumbidgee River during irrigation flow releases. Mar Freshwater Res 56:227–241

Walsh CJ, Roy AH, Feminella JW, Cottingham PD, Groffman PM, Morgan RP (2005) The urban stream syndrome: current knowledge and the search for a cure. J N Am Benthol Soc 24:706–723

Wenger SJ, Roy AH, Jackson CR, Bernhardt ES, Carter TL, Filoso S et al (2009) Twenty six key research questions in urban stream ecology: an assessment of the state of the science. J N Am Benthol Soc 28(4): 1080–1098

Winkler LW (1888) Die besistimmung des in wasser gelosten sanerstoffen. Berichte der deutsche chemischen geschlschaft 21: 2542–2855

Young RG, Matthaei CD, Townsend CR (2008) Organic matter breakdown and ecosystem metabolism: functional indicators for assessing river ecosystem health. J N Am Benthol Soc 27:605–625

Yvon-Durocher G, Caffrey JM, Cescatti A, Dossena M, del Giorgio P, Gasol JM, Montoya JM, Pumpanen J, Staehr PA, Trimmer M, Woodward G, Allen AP (2012) Reconciling the temperature dependence of respiration across timescales and ecosystem types. Nature 487:472–476